



INSTITUTE FOR DEFENSE ANALYSES

Broadband Performance Limits of Ultra-Thin Lenses

Jeremy A. Teichman

May 2021

Approved for public release;
distribution is unlimited.

IDA Document NS D-22662

Log: H 21-000170

INSTITUTE FOR DEFENSE ANALYSES
4850 Mark Center Drive
Alexandria, Virginia 22311-1882



The Institute for Defense Analyses is a nonprofit corporation that operates three Federally Funded Research and Development Centers. Its mission is to answer the most challenging U.S. security and science policy questions with objective analysis, leveraging extraordinary scientific, technical, and analytic expertise.

About This Publication

This work was conducted by the Institute for Defense Analyses (IDA) under contract HQ0034-19-D-0001, Project DA-2-4291, "EXTREME Optics," for the Defense Sciences Office (DSO) of the Defense Advanced Research Projects Agency (DARPA). The views, opinions, and findings should not be construed as representing the official position of either the Department of Defense or the sponsoring organization.

For More Information

Jeremy A. Teichman, Project Leader
jteichma@ida.org, (703) 578-2975

Leonard J. Buckley, Director, Science and Technology Division
lbuckley@ida.org, (703) 578-2800

Copyright Notice

© 2021 Institute for Defense Analyses
4850 Mark Center Drive, Alexandria, Virginia 22311-1882 • (703) 845-2000.

This material may be reproduced by or for the U.S. Government pursuant to the copyright license under the clause at DFARS 252.227-7013 (Feb. 2014).

INSTITUTE FOR DEFENSE ANALYSES

IDA Document NS D-22662

**Broadband Performance Limits of
Ultra-Thin Lenses**

Jeremy A. Teichman

Broadband performance limits of ultra-thin lenses

JEREMY TEICHMAN*

Institute for Defense Analyses, 4850 Mark Center Drive, Alexandria, VA 22311, USA
**jteichma@ida.org*

Abstract: Thin lenses of sufficient diameter and focusing power cannot fully compensate for variation in free-space time of flight to maintain and focus an intact wavefront and instead combine successive wavefronts. The limited temporal coherence of broadband light reduces the effectiveness of such interference. Using equivalent medium theory and scalar diffraction we exploit time-domain analysis to show that the temporal coherence of illumination imposes hard limits on the performance of thin lenses as measured by the Strehl ratio. These limits apply equally to diffractive optical elements and metalenses.

© 2021 Optical Society of America under the terms of the [OSA Open Access Publishing Agreement](#)

1. Introduction

Lenses based on diffractive optical elements (DOEs) and metalenses control phase or amplitude of light across an aperture to focus the light via engineered constructive interference of diffracted waves at the focal point. Both work by effectively delaying the wavefront in a spatially varying fashion. Thin lenses of sufficient diameter and focusing power, however, cannot fully compensate for variation in free-space time of flight to maintain and focus an intact incident wavefront. Instead, they combine successive wavefronts. Broadband light, due to its limited temporal coherence, reduces the effectiveness of such interference. We represent lenses using equivalent medium theory and scalar diffraction and show that temporal coherence of the illumination imposes hard limits on the performance of lenses as measured by the Strehl ratio. The same bound will apply to DOEs and metalenses, including those using dispersion engineering.

Recent papers have described DOEs and metalenses with broadband focusing effects [1–7]. Others have used frequency-domain approaches to analyze diffractive lens performance [8–12]. A chief advantage of the time-domain approach reported here is that it separates the influences on performance of the properties of the illumination, the constraints of lens construction, and the optical requirements. Here, we explore the bounds of performance of thin lenses under broadband light using temporal coherence and show computations for band-limited white light. The model and bounds apply equally well to DOEs and metalenses, including dispersion-engineered metalenses such as described in [3]. Presutti and Monticone analyzed time-bandwidth considerations in computing the maximum size of broadband metalenses near the diffraction limit [13] in the region well-approximated by the extended Marechal approximation [14]. We consider far larger lenses potentially distant from the diffraction limit. The general construct in [13] of treating a broadband lens as attempting to compensate for time-of-flight differences applies to our analysis as well, but we quantify and bound the consequences of failing to fully compensate, while [13] analyzes the conditions under which nearly full compensation is possible.

We model the lens as a radially symmetric thin layer producing a time delay τ as a function of radial coordinate ρ . A given lens material/manufacturing system will provide a maximum span of admissible time delays T . Ignoring a piston mode, we express the constraint as requiring $|\tau| \leq T/2$. In the case of a diffractive element, under the approximations of effective medium theory and scalar diffraction, this would correspond to a dispersionless material with refractive

index n and thickness varying by up to $Tc/(n-1)$, where c is the speed of light in a vacuum. This treatment applies equally well to discrete DOEs composed of annular grooves on a substrate or continuously varying kinoform lenses. A metalens can be similarly described as having an achievable span of effective time delays (with or without dispersion engineering). In what follows, we use the Huygens-Fresnel formulation to compute a bound for the Strehl ratio at the focal point.

2. Strehl ratio at the focal point

For a plane-wave normally incident on a radially symmetric planar aperture with diameter D and effective optical path delay $\tau(\rho)$ (refer to Fig. 1), the Huygens-Fresnel formulation including obliquity for the resulting scalar field at an on-axis focal point a distance f from the aperture is [15]

$$E(t) = \int_0^{D/2} d\rho \frac{f\rho}{c(f^2+\rho^2)} \frac{\partial}{\partial t} E_0 \left(t - \tau(\rho) - \frac{\sqrt{f^2+\rho^2}}{c} \right), \quad (1)$$

where $E_0(t)$ is the scalar field of the incident plane-wave. For convenience, we change variables to $\xi \equiv \sqrt{f^2 + \rho^2}/c$ (the free-space time-of-flight) and switch notation such that $\tau(\xi)$ is the effective optical path delay at the aperture location now defined by ξ .

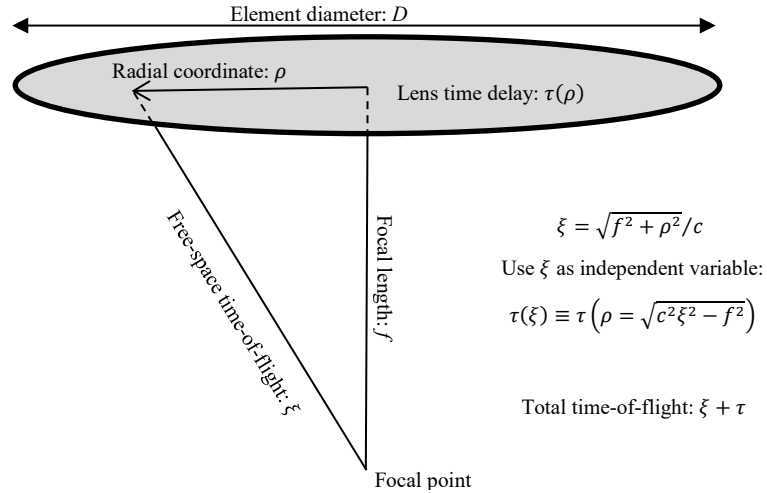


Fig. 1. System schematic of radially-symmetric thin lens of diameter D and focal length f characterized by its effective time delay τ , where τ can equivalently be given as a function of the radial coordinate ρ or as a function of the free-space time of flight ξ associated with a given point on the aperture.

We also define the free-space optical path in units of the center wavelength λ_0 along the central ray and marginal ray, respectively, as

$$\ell_1 \equiv \sqrt{f^2 + \frac{1}{4}D^2}/\lambda_0 \quad \text{and} \quad \ell_2 \equiv f/\lambda_0, \quad (2)$$

leading to

$$E(t) = \frac{f}{c} \int_{\ell_2 \lambda_0/c}^{\ell_1 \lambda_0/c} \frac{d\xi}{\xi} \frac{\partial}{\partial t} E_0(t - \tau(\xi) - \xi). \quad (3)$$

Ignoring uniform time delays (piston mode), a diffraction-limited lens has $\tau_{DL}(\xi) = -\xi$ and $E_{DL}(t) = \frac{f}{c} \ln \left(\frac{\ell_1}{\ell_2} \right) \frac{\partial}{\partial t} E_0(t)$. The Strehl ratio Φ is given by the ratio of the intensity of the scalar field at the focus of a lens relative to the intensity of a diffraction-limited lens of the same size,

$$\Phi = \frac{\langle E(t)E^*(t) \rangle}{\langle E_{DL}(t)E_{DL}^*(t) \rangle}, \quad (4)$$

where the * indicates complex conjugation and angle brackets indicate expected value in the sense of statistical optics. In Section 5 of this paper, we discuss nuances of various definitions of Strehl ratio. Using (3) in (4) leads to

$$\Phi = \left(\ln \frac{\ell_1}{\ell_2} \right)^{-2} \int_{\ell_2 \lambda_0/c}^{\ell_1 \lambda_0/c} \frac{d\xi}{\xi} \int_{\ell_2 \lambda_0/c}^{\ell_1 \lambda_0/c} \frac{d\xi'}{\xi'} \frac{\langle \frac{\partial}{\partial t} E_0(t-\tau(\xi)-\xi) \frac{\partial}{\partial t} E_0^*(t-\tau(\xi')-\xi') \rangle}{\langle \frac{\partial}{\partial t} E_0(t) \frac{\partial}{\partial t} E_0^*(t) \rangle}. \quad (5)$$

If we model the incoming plane-wave as statistically stationary, the integrand in (5) reduces to the time-independent complex degree of coherence of the time-derivative of the incoming plane wave (For simplicity, we refer to this as CDC). Following Goodman [15],

$$\gamma'(\Delta t) \equiv \frac{\langle \frac{\partial}{\partial t} E_0(t) \frac{\partial}{\partial t} E_0^*(t+\Delta t) \rangle}{\langle \frac{\partial}{\partial t} E_0(t) \frac{\partial}{\partial t} E_0^*(t) \rangle}, \quad (6)$$

and

$$\Phi = \left(\ln \frac{\ell_1}{\ell_2} \right)^{-2} \int_{\ell_2 \lambda_0/c}^{\ell_1 \lambda_0/c} \frac{d\xi}{\xi} \int_{\ell_2 \lambda_0/c}^{\ell_1 \lambda_0/c} \frac{d\xi'}{\xi'} \gamma'(\tau(\xi) - \tau(\xi') + \xi - \xi'). \quad (7)$$

Equation (7) shows that the Strehl ratio is a function of the lens design strictly via a temporal autocorrelation function of the incident light, and it expresses the fact that a lens focuses light by generating constructive interference at the focal point between light scattered from pairs of points across the aperture.

The time-domain approach is fundamentally equivalent to the more common frequency-domain description. In the limit of long-time averaging, different wavelengths contribute independently to intensity due to the orthogonality of Fourier components, so in (7), the numerator of γ' as defined in (6) could be replaced with a wavelength-by-wavelength Fourier representation. The standard frequency-domain view arises from switching the order of integration to integrate first over space and then over frequency. The wavelength-specific Strehl ratio represents the normalized peak of the monochromatic point-spread function (PSF), which is equivalent to the integral over the wavelength-specific optical transfer function. Care must be taken combining wavelength-specific Strehl ratios, which have wavelength-specific normalizations, into a polychromatic Strehl ratio.

A key advantage of the time-domain approach is that by integrating over the spectrum first, the characteristics of the light are all precomputed, and the effects of the illumination and the lens can be treated separately. The frequency-domain approach computes the effect of the lens and illumination together for every possible wavelength and then assimilates the constitutive spectrum.

3. Limits of performance

The limited range of element time delays restricts the domain of the autocorrelation accessible for a given pair of rings on the aperture (ξ, ξ') . In particular, $|\tau(\xi) - \tau(\xi')| \leq T$. The best achievable lens would be the maximum of (7) over all lens designs $\tau(\xi)$. Currently, inverse-design procedures, like that described in [1], attempt to iteratively optimize a given design. However, the resulting prescriptions are not easily characterized nor are they proven globally optimal. To our knowledge, there is no known and proven globally optimal design, which is why the bounds sought in this paper would be instructive.

To identify performance bounds to all designs, we look at potentially inconsistent designs by independently optimizing $\tau(\xi)$ and $\tau(\xi')$. In effect, for each aperture ring ξ , we credit maximal constructive interference at the focus from all other aperture rings ξ' , regardless of mutual compatibility with constructive interference between those other rings. In other words,

$\tau(\xi')$ in the inner integral in (7) will in general be a different function for each value of ξ in the outer integral.

Intensity is a linear sum of contributions, each from the conjugate product of the scalar field at a pair (including degenerate pairs) of aperture points. Consider three points on the aperture with scalar fields A, B, and C. The intensity computed from the Huygens-Fresnel integral adds the contributions AA^* , AB^* , AC^* , BA^* , etc. A real design only has three degrees of freedom in these contributions, namely the element properties at A, B, and C. If we ignore the fact that A must have the same properties when counting the contributions from AB^* and CA^* , we may be able to improve apparent performance even though such an element is unrealizable. The element with AB^* and CA^* independently optimized is guaranteed to perform at least as well as the element where A is constrained by reality to be identical in AB^* and CA^* . In the appendix we consider a bound based on independently optimizing the contribution of every pair of points, treating AA^* , AB^* , BA^* , etc. each as a fully independent variable. In what follows, we reimpose a measure of consistency and require A to be the same for AA^* , AB^* , and AC^* , but allow it to differ for BA^* and CA^* .

Because these various unphysical optimization spaces include the real design space, any optimum over the unphysical spaces is guaranteed to perform at least as well as the optimum over the realizable design space. There is no guarantee that the bounds will not wildly overpredict performance—they could be very loose—but they cannot underpredict performance. In other words, the bounds are guaranteed to be rigorous but not tight. Later in the paper, we will show comparisons between the bounds and published elements and observe that the bounds are all within an order of magnitude of practical performance and often much closer.

Returning to the mathematical derivation, from (7), the Strehl ratio

$$\Phi \leq \left(\ln \frac{\ell_1}{\ell_2} \right)^{-2} \int_{\ell_2 \lambda_0/c}^{\ell_1 \lambda_0/c} \frac{d\xi}{\xi} \max_{\tau_1} \int_{\ell_2 \lambda_0/c}^{\ell_1 \lambda_0/c} \frac{d\xi'}{\xi'} \max_{\tau_2} \gamma'(\tau_1 - \tau_2 + \xi - \xi'), \quad (8)$$

where, ignoring the piston mode, the maxima are over $-T/2 \leq \tau \leq T/2$. τ_1 and τ_2 are the time delays imposed by the element at ξ and ξ' . Eq. (8) exhibits the separation of contributions, where γ' captures the illumination conditions, τ_1 and τ_2 capture the design constraints, and ℓ_1 and ℓ_2 capture the optical requirements. As described above, this bound represents an unachievable design because the profile $\tau_2(\xi')$ is not the same for every ξ . Let $\zeta \equiv \xi' - \xi - \tau_1$. Changing variables and exploiting the fact that γ' is an even (and real) function for illumination with symmetric expected power spectral density,

$$\Phi \leq \left(\ln \frac{\ell_1}{\ell_2} \right)^{-2} \int_{\ell_2 \lambda_0/c}^{\ell_1 \lambda_0/c} \frac{d\xi}{\xi} \max_{\tau_1} \int_{\ell_2 \lambda_0/c - \xi - \tau_1}^{\ell_1 \lambda_0/c - \xi - \tau_1} \frac{d\zeta}{\zeta + \xi + \tau_1} G(\zeta, T), \quad (9)$$

where we define a function $G(\zeta; T) \equiv \max_{|\tau| \leq T/2} \gamma'(\zeta + \tau)$. $G(\zeta; T)$ is a function of only the light's temporal coherence and the lens's range of time delays. $G(\zeta; T)$ is the maximum CDC over a sliding window centered around $\Delta t = \zeta$ with width T .

As long as $G(\zeta; T)$ is strictly non-negative, which it should be so long as the lens has the ability to generate a 2π phase shift at the center frequency, the integrand in (9) is non-negative, and the integrity of the bound can be maintained while eliminating dependence of the inner integral on τ_1 by expanding the limits of the inner integral to the maximum possible extent and using the minimum value of τ_1 in the denominator. Thus,

$$\Phi \leq \left(\ln \frac{\ell_1}{\ell_2} \right)^{-2} \int_{\ell_2 \lambda_0/c}^{\ell_1 \lambda_0/c} \frac{d\xi}{\xi} \int_{\ell_2 \lambda_0/c - \xi - T/2}^{\ell_1 \lambda_0/c - \xi + T/2} \frac{d\zeta}{\zeta + \xi - T/2} G(\zeta; T). \quad (10)$$

Note that for large lenses and broadband light, the loss of tightness of the bound in this step is likely to be small because first, the inflation of the integral limits takes place mostly at large optical path differences where the CDC is small, and second, $T \ll \zeta + \xi$. For small lenses, we can define an alternate bound described in the appendix, equally rigorous but without this

particular relaxation of the bounds. Bounds reported here represent the tighter of the two. Let us define

$$\mu \equiv Tc/\lambda_0, g(\psi; \mu) = G(\psi\lambda_0/c; \mu\lambda_0/c), \quad (11)$$

where μ is the harmonic order of the lens (the maximum optical path delay achievable by the lens in units of λ_0). Using (11), the nondimensional form of (10) (including converting the dummy variable ξ in the first integral to nondimensional form) is

$$\Phi \leq \left(\ln \frac{\ell_1}{\ell_2}\right)^{-2} \int_{\ell_2}^{\ell_1} \frac{d\xi}{\xi} \int_{\ell_2 - \xi - \mu/2}^{\ell_1 - \xi + \mu/2} \frac{d\psi}{\psi + \xi - \mu/2} g(\psi; \mu). \quad (12)$$

Switching the order of integration in (12) and integrating with respect to ξ , leads to

$$\Phi \leq \left(\ln \frac{\ell_1}{\ell_2}\right)^{-2} \left\{ \int_{-\mu/2}^{\mu/2} \frac{d\psi}{\psi - \mu/2} \ln \frac{\ell_1(\psi - \mu/2 + \ell_2)}{\ell_2(\psi - \mu/2 + \ell_1)} + \int_{\mu/2}^{\ell_1 - \ell_2 + \mu/2} d\psi g(\psi; \mu) \left[\frac{1}{\psi - \mu/2} \ln \frac{(\ell_1 - \psi + \mu/2)(\ell_2 + \psi - \mu/2)}{\ell_1 \ell_2} + \frac{1}{\psi + \mu/2} \ln \frac{(\ell_1 - \psi - \mu/2)(\ell_2 + \psi - \mu/2)}{\ell_1(\ell_2 - \mu)} \right] \right\}, \quad (13)$$

with details of the derivation of (13) from (12) given in the appendix. For a given illumination condition, (13) can be evaluated numerically to find the Strehl ratio upper bound.

For insight, let us look at the terms in (13). The first term in the $\{\}$ in (13) represents the refractive contribution to focusing. The harmonic order μ places a limit on the region of the lens that can contribute to coherent superposition of light waves without resorting to phase folding. The refractive contribution consists of the incoherent superposition of all such regions. Hence, the refractive contribution comes from assuming $g(\psi; \mu) = 0$ outside of $[-\mu/2, \mu/2]$.

The second term in the $\{\}$ in (13) represents the diffractive contribution, which comes from coherent superposition of successive wavefronts from different parts of the aperture and relies on phase folding. For a given temporal coherence of light, $g(\psi; \mu)$ quantifies the maximum possible diffractive contribution as a function of ψ , the number of waves of correction required, and μ , the available correction without phase folding.

Next, we look at some limiting approximations. If the obliquity factor $\chi = \frac{f}{\sqrt{f^2 + \rho^2}}$ can be neglected, (13) reduces to

$$\Phi \leq \frac{\mu}{\Delta\ell} + 2 \frac{\mu}{\Delta\ell} \int_{1/2}^{\Delta\ell/\mu + 1/2} d\eta \left(1 - \frac{\mu}{\Delta\ell} \left(\eta - \frac{1}{2}\right)\right) g(\mu\eta; \mu) \quad (14)$$

where $\Delta\ell \equiv \ell_1 - \ell_2 = \frac{D}{\lambda_0} \left(\sqrt{f\#^2 + \frac{1}{4}} - f\#\right)$, $f\# \equiv f/D$, and $\eta \equiv \psi/\mu$. If obliquity is significant, but the illumination is sufficiently temporally incoherent that $g(\psi; \mu) \approx 0$ for $|\psi| > \mu/2$, then (13) can be approximated as

$$\Phi \lesssim \mu \left(\ln \frac{\ell_1}{\ell_2}\right)^{-2} \left(\frac{1}{\ell_2} - \frac{1}{\ell_1}\right), \quad (15)$$

as long as $f \gg cT$, by using

$$\int_{-\mu/2}^{\mu/2} d\psi \int_{\ell_2}^{\ell_1} \frac{d\xi}{\xi} \frac{1}{\psi + \xi - \mu/2} \approx \int_{-\mu/2}^{\mu/2} d\psi \int_{\ell_2}^{\ell_1} \frac{d\xi}{\xi^2}. \quad (16)$$

When the obliquity factor can be neglected and illumination is sufficiently incoherent, (15) reduces to

$$\Phi \lesssim \frac{\mu}{\Delta\ell}. \quad (17)$$

In the limit of high $f\#$, (15) and (17) both become

$$\Phi \lesssim 8f\#\mu \frac{\lambda_0}{D}. \quad (18)$$

Note that the approximations in (15), (17), and (18) treat the lens as a series of independent annular lenses incoherently combined at a common focus.

The scaling term $\Delta\ell/\mu$, apparent in (14) and (17), is the minimum number of coherent subapertures. The refractive contribution to the Strehl ratio will scale with the inverse of the number of incoherently combined refractive subapertures.

4. Band-limited white light

As a concrete example of the bounds derived in the previous section, we treat band-limited white light with center frequency ν_0 and bandwidth $\Delta\nu$. For band-limited white light with $B \equiv \Delta\nu/\nu_0$,

$$\gamma'(\Delta t) = \frac{1}{2\pi\left[2 + \frac{1}{6}B^2\right]B\nu_0\Delta t} \left\{ \sin(\pi B\nu_0\Delta t) \left[\cos(2\pi\nu_0\Delta t) \left(4 + B^2 - \frac{2}{\pi^2(\nu_0\Delta t)^2} \right) - \frac{4}{\pi\nu_0\Delta t} \sin(2\pi\nu_0\Delta t) \right] + \cos(\pi B\nu_0\Delta t) \left[4B \sin(2\pi\nu_0\Delta t) + \frac{2B}{\pi\nu_0\Delta t} \cos(2\pi\nu_0\Delta t) \right] \right\}, \quad (19)$$

which can be derived from a Fourier representation by analytically integrating $\gamma'(\Delta t) = \int d\nu \nu^2 \exp(i2\pi\nu\Delta t) / \int d\nu \nu^2$ over the bandwidth. In the limit of narrow bandwidth,

$$\gamma'(\Delta t) = \cos(2\pi\nu_0\Delta t) \text{sinc}(B\nu_0\Delta t). \quad (20)$$

Fig. 2 shows $g(\psi; \mu)$ for fractional bandwidth $B = 0.1, 0.5, 1$ and lens harmonic order $\mu = 1, 5, \text{ and } 10$, along with $\gamma'(\psi)$, which corresponds to $g(\psi; 0)$. Note that for harmonic order less than the reciprocal fractional bandwidth, there are local minima in $g(\psi; \mu)$, indicating that regions with greater free-space optical-path difference may sometimes contribute more to constructive interference at the focus than those with less optical-path difference. In other words, there may be regions whose diffractive contributions generate destructive interference.

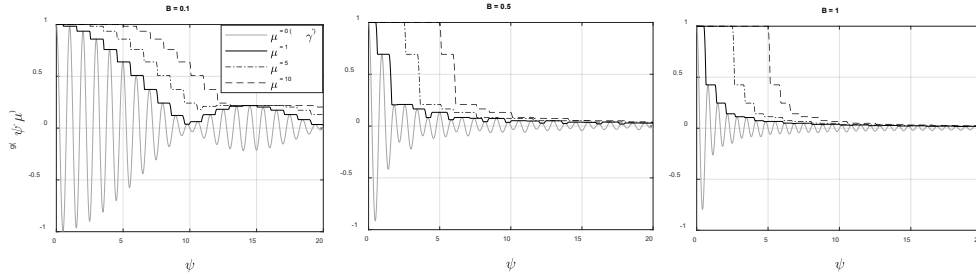


Fig. 2. For band-limited white light, the figure shows $\gamma'(\psi/v_0)$, the CDC, where $\psi = \nu_0\Delta t$, along with $g(\psi; \mu)$, the sliding maximum of $\gamma'(\psi/v_0)$ over the interval $[\psi - \frac{1}{2}\mu, \psi + \frac{1}{2}\mu]$, where μ is the harmonic order of the lens. Note that $\gamma'(\psi/v_0) = g(\psi; 0)$. From left to right, the panels show fractional bandwidth $B = \Delta\nu/\nu_0$ of 0.1, 0.5, and 1. Each panel shows results for $\mu = 1, 5, \text{ and } 10$.

Fig. 3 shows the upper bound Strehl ratio for lenses of various sizes, harmonic orders, bandwidths, and f# under white-light illumination centered in the visible band around $\lambda_0 = c/\nu_0 = 510 \text{ nm}$. The full band from 400 to 700 nm corresponds to a fractional bandwidth of $B = 0.55$. The Strehl ratio upper bound decays a little more slowly than the reciprocal of the lens diameter, which would be the scaling predicted by (18).

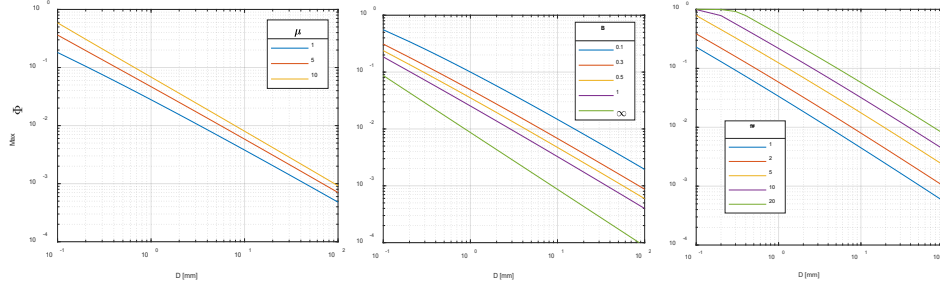


Fig. 3. Upper bound for Strehl ratio as a function of lens diameter. (a) Various harmonic orders μ , for $f/1$ and band-limited white light in the visible spectrum from 400 to 700 nm corresponding to $B = 0.55$ and $\lambda_0 = 510$ nm (b) Various fractional bandwidth B , for $f/1$, $\mu = 2$, and $\lambda_0 = 510$ nm (c) Various $f\#$, for $\mu = 2$, $B = 0.55$, and $\lambda_0 = 510$ nm. In the far upper left corner of (c), the kinks in the curves indicate where the alternate bound from the appendix transitions to the bound in the main body of this paper.

We intended to compare these bounds with the performance of lenses in the recent literature. However, we found very few lenses making use of diffractive optics or metasurfaces with $\Delta\ell/\mu$ significantly greater than one. In other words, there were few lenses at low enough $f\#$ and large enough diameter to require a significant number of subaperture zones. References [3] and [13] compiled lists of recently published metalens designs. We computed the effective $\Delta\ell/\mu$ for all the designs and found that they range from 0.3 to 8.5. This fits with their examination of the bandwidth limits of near-diffraction-limited lenses. Meem et al. have published results for a millimeter-scale fast broadband DOE [1]. Table 1 shows results for the lens from [1] as well as those cataloged by [3] and [13] for which $\Delta\ell/\mu > 2$, $\mu \geq 1$, $\ell_2 > \mu$, and $D/\lambda_0 \geq 50$. Where available, we compare to reported Strehl ratios for the same lenses. For comparison of the bound to a physically realistic design, we also show the Strehl ratio for a dispersionless kinoform lens of order $m = \lfloor \mu \rfloor$ with $M = \lceil \Delta\ell/\lfloor \mu \rfloor \rceil$ zones, which, from a modified version of (7) neglecting obliquity, is

$$\Phi = \frac{1}{M^2} \sum_{p=1..M} \sum_{q=1..M} \gamma'((p-q)m/v_0). \quad (21)$$

Table 1. Survey of published lenses

Diameter (mm)	Focal length (mm)	Band (μm)	Harmonic order	$\frac{\Delta\ell}{\mu}$	Strehl bound	Kinoform Strehl	Reported Strehl	Source
3.145	5	0.45–1	2.6	128	0.02	0.0032	0.0075 ^a	[1]
0.44	11	0.47–0.67	1.68	2.3	0.91	0.64	0.1 ^a	[2]
0.2	0.485	0.49–0.55	2.66	7.2	0.62	0.39	<0.15 ^b	[4]
0.1	0.2	1.3–1.65	1.47	2.8	0.93	0.71	0.3 ^a	[5]
0.1	0.03	1.2–1.4	2.9	7.6	0.54	0.26	?	[5]
0.366	1	0.45–0.75	3.25	8.5	0.24	0.07	<0.22 ^b	[6]
0.014	0.0035	0.45–0.75	1.56	4.8	0.56	0.21	<0.34 ^b	[6]
0.24	0.656	1.45–1.59	1.82	3.9	0.95	0.87	~0.4–0.8	[7]

^aStrehl ratios reported in [1] (0.75), [2] (0.94), and [5] (0.9) are too high to be compatible with reported focusing efficiencies of ~12%, ~10%, and ~35%, respectively. The reported Strehl ratios may be normalized with respect to the focal efficiency. As used in this paper, the reported Strehl ratios with their associated focusing efficiencies would require spot sizes far smaller than the diffraction limit to achieve the required peak value while capturing a smaller amount of power. The Strehl ratios presented in the table undo the presumed normalizations. For the [1] lens, from supplemental figure S16 in that paper, it appears that the circled power within a diffraction-limited spot (and the paper claims a nearly-diffraction-limited spot size) is closer to 1% of that expected from a diffraction-limited lens. If so, the adjusted de-normalized Strehl ratio of 0.09 based on their reported focusing efficiency is still too high. A

normalized Strehl ratio reported relative to the 1% focusing efficiency would be associated with a standard Strehl ratio of 0.0075, which is the value used in the table above. If total transmission is low for [2] or [5], using the efficiency the way we have could underestimate the transmission-normalized Strehl ratio. For [1], the encircled power plot from which we drew the 1% efficiency number asymptotes to 100%, so any transmission losses are already included.

^b[4] and [6] report focusing efficiencies for these three lenses. The Strehl ratio can be approximately capped at the efficiency as long as the true PSF is not more sharply peaked than the diffraction-limited PSF. In [4], the nearly diffraction-limited spot size improves the efficiency-based estimate because there is little additional Strehl ratio degradation due to spreading of power over a larger focal spot. As in the previous note, poor transmission could cause efficiency-based estimates to underestimate transmission-normalized Strehl ratios.

5. Discussion

Although all definitions of the Strehl ratio with which we are familiar use the actual intensity at the focal spot relative to the intensity produced by a perfect lens, we have encountered a number of different normalization standards. In our usage, we normalize relative to the focal intensity of a perfect lens of the same aperture with 100% transmission. Some authors normalize with respect to a perfect lens of the same total transmission as the real lens—this is the value attained by integrating the area under the modulation transfer function, which is normalized to have a value of one at zero spatial frequency (corresponding to total transmission). Both these definitions preserve the connection between Strehl ratio and contrast. Some authors normalize the Strehl ratio with respect to a perfect lens of the same aperture with the same amount of total energy in the focal spot. This definition severs the connection with contrast because it normalizes out widely diffused light, but it preserves some connection to the spot size because, for the same total focused energy, a higher peak intensity corresponds to a tighter spot. The focusing efficiency (fraction of incident light confined to the focal spot) connects this measure of Strehl ratio to more classical definitions.

When dealing with refractive lenses, one would not expect much difference between the definitions because transmission is typically high, and loss of contrast is typically due to expansion or smearing of the focal spot. In diffractive optics and meta-optics, much loss of contrast can be due to zeroth-order diffraction and widely scattered light, so substantial loss of contrast can occur while retaining a near-diffraction-limited focal spot. With these lenses, the different Strehl ratio definitions can yield widely varying values with quite different interpretations and performance implications.

Many metalenses utilize design libraries with more degrees of freedom than a typical diffractive element, allowing simultaneous tuning of phase delay and dispersion. Dispersion engineering refers to the combined use of these freedoms. In the framework of this analysis, the equivalent μ of a metalens is proportional to the largest effective time delay possible at the center wavelength while controlling dispersion. This is given by the maximum achievable group delay the meta-element library is capable of while retaining 2π phase delay capability. The metalens's equivalent harmonic order is given by $\mu = \nu_0 \frac{\partial \phi}{\partial \omega}$, where $\frac{\partial \phi}{\partial \omega}$ is the maximum group delay with 2π phase-delay capability. With this definition of μ , the bounds derived here are equally applicable to metalenses.

In this paper, we neglect chromatic dispersion in the bounds. Can dispersion increase the performance in a way that undermines the rigor of the bounds? If not, can a tighter set of bounds be derived by accounting for dispersion behavior? We believe that dispersion will reduce both the refractive and diffractive performance of the lens, such that the bounds derived above remain rigorous. In this context, we construe refractive performance as the contribution from subapertures over which the free-space path difference is fully compensated (without phase folding and neglecting dispersion) by the lens and diffractive performance as the contribution from constructive interference between such subapertures requiring phase folding.

Let us treat the refractive contribution first. With dispersion-free behavior, the lens is able to fully compensate for free-space optical-path differences within the refractive capacity of the material system ($g(\psi; \mu) = 1$ for $|\psi| < \mu/2$). Any dispersion would cause the CDC to degrade for any $\psi \neq 0$, although for thin lenses, the dispersive effect is likely to be small. Introducing

the Abbe number $V \equiv (n(\nu_0) - 1)/\Delta n$, where Δn is the span of refractive index across the waveband, the maximum dispersive contribution to phase error at the edge of the waveband would be $\frac{\pi\mu}{2V}(2 + B)$. For fractional bandwidth $B \ll 2$, this is approximately $\frac{\pi\mu}{V}$. When the harmonic order of the lens is much less than the Abbe number $\mu \ll V$, there is little contribution of dispersion to reducing the refractive contribution of the lens.

For the diffractive contribution, we consider what happens at phase jumps of 2π at the center wavelength. The dispersive effect can be thought of as analogous to expanding the bandwidth. A 2π phase jump at the center wavelength corresponds, at other wavelengths, to some deviation from 2π , increasing with increasing deviation from the center wavelength. Shorter wavelengths will experience a larger than 2π phase jump, and longer wavelengths will experience a smaller than 2π phase jump. This occurs because the same jump in time delay will correspond to a larger number of wavelengths of optical path at the shorter wavelengths. Dispersion, which increases the index at shorter wavelengths, will further increase the phase jump at short wavelengths and further decrease the phase jump at longer wavelengths. Thus, the spread of phase jumps experienced over the spectrum will increase just as it would for higher bandwidth, and the CDC will decrease for light at the focal point from aperture points on opposite sides of a phase jump.

The phase discrepancy between the center frequency and the edge of the band across jumps of maximum size can be expressed as $\Delta\phi = \pi\mu \left[B + \frac{B+2}{2V} \right]$, where the second term in the brackets represents the marginal contribution to phase error from dispersion. Thus, for $B \ll 2$, the dispersive-phase-error contribution to diffractive focusing will be at most $\Delta\phi \approx \pi\mu/V$. As long as $B \gg 1/V$, however, decoherence due to broadband illumination will dominate diffractive losses before dispersion begins to contribute meaningfully. For higher order diffractive contributions accumulated over numerous phase jumps, the phase discrepancy for M such jumps will be $\Delta\phi = M\pi\mu \left[B + \frac{B+2}{2V} \right]$. Accounting for the maximum phase discrepancy over the entire lens, $\Delta\phi = \pi(\Delta\ell - \mu) \left[B + \frac{B+2}{2V} \right]$. In either case, broadband rather than dispersive losses are likely to dominate diffraction losses for $B \gg 1/V$ for reasonable Abbe number and bandwidth.

Although dispersion-engineered metalenses may be able to approximate dispersion-free behavior, unless a DOE would operate in a regime where material dispersion effects significantly affect the refractive contribution, we would not expect significant differences between DOEs and metalenses for similar designs and similar harmonic orders. In sum, despite ignoring dispersion, since dispersion should detract from performance, we believe our bounds will remain rigorous, and since dispersive effects are expected to be small, we believe the tightness of the bounds will not suffer much.

Nevertheless, one could construct a version of $g(\psi; \mu)$ accounting for dispersion, representing the best achievable CDC given material/manufacturing constraints as a function of free-space optical-path difference. In relation to the stepped appearance of $g(\psi; \mu)$ in Fig. 2, we would expect the dispersive effect on refraction to turn the level steps into sloped ones and the dispersive effect on diffraction to create larger jumps between the steps as shown at exaggerated scale in Fig. 4.

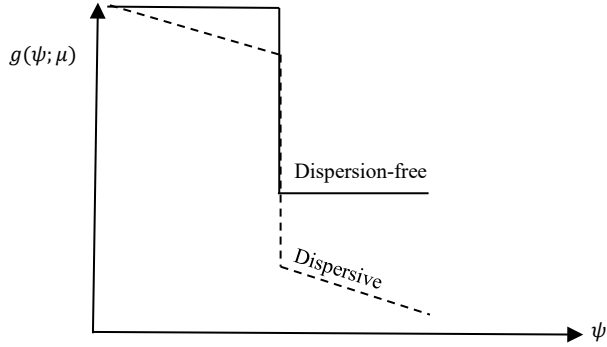


Fig. 4. Qualitative effect of dispersion on best achievable CDC $g(\psi; \mu)$.

We also neglected off-axis effects and polarization in our analysis. For a system optimized for on-axis Strehl ratio, off-axis performance would likely be worse than on-axis. Shadowing effects, reflective losses, effective aperture size, and obliquity losses would all rise off-axis. Likewise, polarization sensitivity would not provide an opportunity for better optimization, but a design optimized for designated polarization conditions would likely perform more poorly under off-nominal polarization conditions. We have not considered developing bounds for performance off-axis or under various polarization assumption, but we believe that the bounds reported here would apply under such circumstances.

Off-axis performance and polarization-sensitive performance are important conditions differentiating metalenses from DOEs. Metalenses may have independently optimizable polarization and angle-dependent behavior, in which case they might be able to outperform DOEs under the right circumstances. Metalenses without independently optimizable angle and polarization behavior could significantly underperform relative to DOEs. Nothing in this analysis sheds light on these differences. Any bounding of performance under these off-nominal conditions would require detailed information about the limits of design freedom of the metalenses.

A principal advantage of the approach presented in this paper is that it allows separation of the light properties and lens prescription. The CDC of broadband light γ' can be precomputed and depends only on the properties of the illumination. Via the maximum time delay achievable by a DOE or metalens, γ' can then easily be converted into the maximum achievable CDC for any required optical path difference. At that stage, the material system (design constraints) and light properties have been folded into the function $g(\psi; \mu)$. Then, the maximum Strehl ratio for any given focal length and aperture size can be computed as an integral over the function $g(\psi; \mu)$, where the optical requirements enter via ℓ_1 and ℓ_2 . It is this separation that enables the bounding by allowing direct treatment of the broadband performance of the lens.

In frequency-domain approaches, the performance of the element is computed first as a function of the illumination wavelength and then integrated over the spectrum. This leaves no clear way to produce useful bounds—because a DOE can theoretically achieve perfect monochromatic performance, optimizing one wavelength at a time would produce a perfect lens. DOE designers must either optimize at one particular wavelength or use inverse-design procedures where they iteratively tweak the design and compute the broadband (or discrete multi-wavelength) performance by integrating over the spectrum. A time-domain approach like that described here might find practical application in speeding up inverse-design algorithms for broadband-diffractive elements using (7) with a precomputed γ' .

Intensity is a nonlinear function of the scalar field over the aperture, but it is a linear function of the Hermitian products of scalar fields at pairs of aperture positions (see (5)). Because the intensity can be computed as a weighted sum of these products (weights depend on the spreading of spherical wavelets and obliquity), the total intensity is bounded by the weighted

sum over the maximum possible intensity contribution of each pair, which is proportional to $g(\psi; \mu)$. Pairs of aperture points cannot be designed independently—in reality, each aperture point is designed, and the pairs come from all combinations of points. In the bound described in the appendix, no additional constraints are placed on the design independence of aperture point pairs. In the bound described in the main body of this paper, the independence of aperture point pairs is partly constrained to tighten the bound relative to realizable designs. In either case, the computed intensity based on independent optimization of aperture point pairs is guaranteed to exceed the performance of any actual lens. The bound is not guaranteed to be tight, but as shown in Table 1, the bound is within a factor of 3 for known, relevant achievable lenses (either a theoretical kinoform design or a specific design from the literature). With that in mind, the bounding performance curves of Fig. 3 show that there are considerable limitations in the expansion of DOEs and metalenses to large aperture and/or low $f\#$ applications. Diffraction-limited focusing may be achievable, but the achievable contrast ratio may be extremely low. While there may be specific applications in which such performance characteristics are acceptable, we feel that it is important to acknowledge these limitations when considering future aspirations for ultra-thin flat lens design.

Funding

Defense Advanced Research Projects Agency, Defense Sciences Office (DARPA/DSO), EXTREME Program.

Acknowledgments

Many discussions with Joe Mait and Predrag Milojkovic helped clarify this paper.

Disclosures

The author declares that there are no conflicts of interest related to this article.

References

1. M. Meem, S. Banerji, A. Majumder, C. Pies, T. Oberbiermann, B. Sensale-Rodriguez, and R. Menon, “Inverse-designed achromatic flat lens enabling imaging across the visible & near-infrared with diameter > 3 mm and $NA=0.3$,” *Appl. Phys. Lett.* **117** 041101 (2020).
2. W.T. Chen, A. Zhu, V. Sanjeev, M. Khorasaninejad, Z. Shi, E. Lee, and F. Capasso, “A broadband achromatic metalens for focusing and imaging in the visible,” *Nature Nanotechnology* **13**, 220–226 (2018).
3. W.T. Chen, A. Zhu, & F. Capasso. Flat optics with dispersion-engineered metasurfaces. *Nat Rev Mater* **5**, 604–620 (2020). <https://doi.org/10.1038/s41578-020-0203-3>.
4. F. Presutti and F. Monticone, “Focusing on bandwidth: achromatic metalens limits,” *Optica* **7**, 624–631 (2020)
5. T. Sean Ross, “Limitations and applicability of the Maréchal approximation,” *Appl. Opt.* **48**, 1812–1818 (2009)
6. J. Goodman, *Statistical Optics* (Wiley-Interscience, 1985).
7. D. Buralli, G. Morris, and J. Rogers, “Optical performance of holographic kinoforms,” *Applied Optics* **28**(5), 976–983 (1989).
8. D. Faklis and G. Morris, “Spectral properties of multiorder diffractive lessons,” *Applied Optics* **34**(14).
9. O. Hignette, J. Santamaria, J. Bescos, “White light diffraction patterns of amplitude and phase zone plates,” *J. Optics* **10**(5), 231–238 (1979).
10. T. Sales and G. Morris, “Diffractive–refractive behavior of kinoform lenses,” *Applied Optics* **36**(1), 253–257 (1997).
11. D. Sweeney and G. Sommargren, “Harmonic diffractive lenses,” *Applied Optics* **34**(14), 2469–2475 (1995).
12. M. Khorasaninejad, Z. Shi, A. Y. Zhu, W. T. Chen, V. Sanjeev, A. Zaidi, and F. Capasso, “Achromatic metalens over 60 nm bandwidth in the visible and metalens with reverse chromatic dispersion,” *Nano Lett.* **17**, 1819–1824 (2017).
13. S. Shrestha, A. C. Overvig, M. Lu, A. Stein, and N. Yu, “Broadband achromatic dielectric metalenses,” *Light: Sci. Appl.* **7**, 85 (2018).
14. N. Mohammad, M. Meem, P. Wang, and R. Menon, “Broadband imaging with one planar diffractive lens,” *Sci. Rep.* **8**, 2799 (2018).
15. E. Arbabi, A. Arbabi, S.M. Kamali, Y. Horie, & A. Faraon. Controlling the sign of chromatic dispersion in diffractive optics with dielectric metasurfaces. *Optica* **4**, 625–632 (2017).

Appendix/supplement

Derivation details

The following provides details of the derivation of (13) from (12) (reproduced here as (22)). Switching the order of integration requires observing that the two integrals represent an integration over a two-dimensional region depicted in Fig. 5.

$$\Phi \leq \left(\ln \frac{\ell_1}{\ell_2}\right)^{-2} \int_{\ell_2}^{\ell_1} \frac{d\xi}{\xi} \int_{\ell_2 - \xi - \mu/2}^{\ell_1 - \xi + \mu/2} \frac{d\psi}{\psi + \xi - \mu/2} g(\psi; \mu). \quad (22)$$

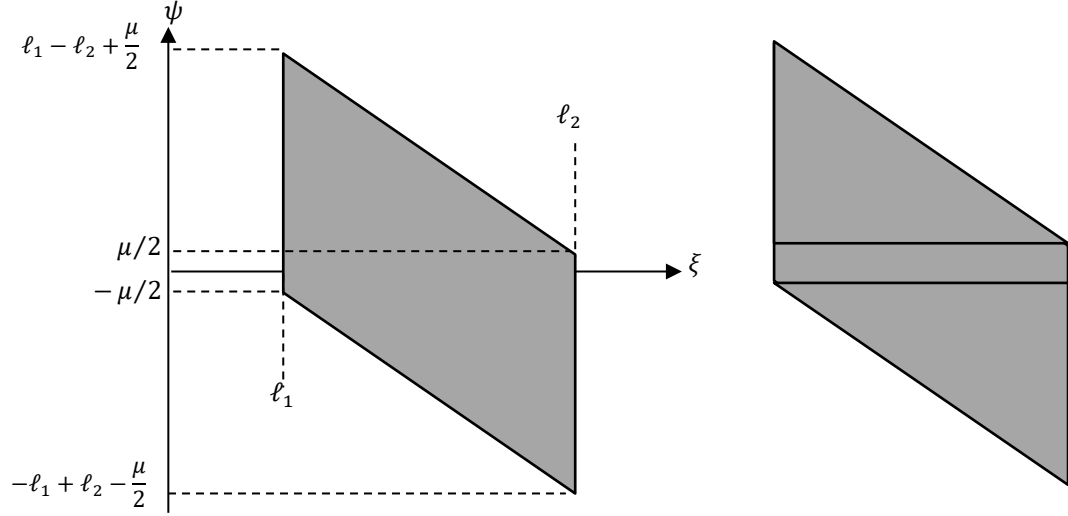


Fig. 5. Schematic of change of order of integration. The domain of integration is shown on the left. In (22), the domain is integrated along vertical strips. Changing the order of integration amounts to switching to integration along horizontal strips in (23), for which the domain must be broken into the three subdomains shown on the right.

Breaking the domain into three subdomains and changing the order of integration in (22) yields

$$\Phi \leq \left(\ln \frac{\ell_1}{\ell_2}\right)^{-2} \left[\int_{\mu/2}^{\ell_1 - \ell_2 + \mu/2} d\psi g(\psi; \mu) \int_{\ell_2}^{\ell_1 - \psi + \mu/2} \frac{d\xi}{\xi} \frac{1}{\psi + \xi - \mu/2} + \int_{-\mu/2}^{\mu/2} d\psi g(\psi; \mu) \int_{\ell_2}^{\ell_1} \frac{d\xi}{\xi} \frac{1}{\psi + \xi - \mu/2} + \int_{\ell_2 - \ell_1 - \mu/2}^{-\mu/2} d\psi g(\psi; \mu) \int_{\ell_2 - \psi - \mu/2}^{\ell_1} \frac{d\xi}{\xi} \frac{1}{\psi + \xi - \mu/2} \right]. \quad (23)$$

Partial fraction expansion of the inner integrand results in

$$\frac{1}{\xi} \frac{1}{\psi + \xi - \mu/2} = \frac{1}{\psi - \mu/2} \left(\frac{1}{\xi} - \frac{1}{\psi + \xi - \mu/2} \right), \quad (24)$$

which can be integrated exactly,

$$\int d\xi \frac{1}{\psi - \mu/2} \left(\frac{1}{\xi} - \frac{1}{\psi + \xi - \mu/2} \right) = \frac{1}{\psi - \mu/2} \left[\ln \xi - \ln \left(\psi + \xi - \frac{\mu}{2} \right) \right] = \frac{1}{\psi - \mu/2} \ln \frac{\xi}{\psi + \xi - \mu/2}. \quad (25)$$

Exact computation of the inner integrals in (23) leads to

$$\Phi \leq \left(\ln \frac{\ell_1}{\ell_2}\right)^{-2} \left[\int_{\mu/2}^{\ell_1 - \ell_2 + \mu/2} \frac{d\psi}{\psi - \mu/2} g(\psi; \mu) \ln \frac{(\ell_1 - \psi + \mu/2)(\psi - \mu/2 + \ell_2)}{\ell_1 \ell_2} + \int_{-\mu/2}^{\mu/2} \frac{d\psi}{\psi - \mu/2} g(\psi; \mu) \ln \frac{\ell_1(\psi - \mu/2 + \ell_2)}{\ell_2(\psi - \mu/2 + \ell_1)} + \int_{\ell_2 - \ell_1 - \mu/2}^{-\mu/2} \frac{d\psi}{\psi - \mu/2} g(\psi; \mu) \ln \frac{\ell_1(\ell_2 - \mu)}{(\psi - \mu/2 + \ell_1)(\ell_2 - \psi - \mu/2)} \right]. \quad (26)$$

Taking the $\psi \rightarrow -\psi$ for the dummy variable in the last integral allows the first and last integrals to be combined. The second integral can be simplified given that $g(\psi; \mu) = 1$ for $|\psi| \leq \mu/2$ because the CDC is always unity for zero time offset, which is achievable if the free-space time-of-flight difference is fully correctable by the element. Together, these lead to (13).

Alternate bound

The bound in the main body of the paper takes one aperture ring at a time and bounds the net intensity contribution from that ring based on a lens optimized for contributions involving that ring. To calculate such a bound, however, a conservative approximation was made between (9) and (10). For small lenses, that approximation can loosen the bound considerably and even generate Strehl ratio bounds greater than one.

Here we consider an alternate bound that relaxes some constraints by independently maximizing the intensity contribution from every pair of rings. Mathematically, this allows τ_1 to vary in the inner integral, whereas the original bound forced τ_1 to remain consistent throughout the inner integral. The alternate bound will underperform the main paper's bound for large apertures but will outperform it for certain small apertures. The alternate bound is always less than one. Results reported in this paper always take the tighter of the two bounds.

Beginning with (8),

$$\Phi \leq \left(\ln \frac{\ell_1}{\ell_2}\right)^{-2} \int_{\ell_2 \lambda_0/c}^{\ell_1 \lambda_0/c} \frac{d\xi}{\xi} \max_{\tau_1} \int_{\ell_2 \lambda_0/c}^{\ell_1 \lambda_0/c} \frac{d\xi'}{\xi'} \max_{\tau_2} \gamma'(\tau_1 - \tau_2 + \xi - \xi'), \quad (27)$$

and relaxing the consistency constraint on τ_1 in the inner integral, we can move the maximization with respect to τ_1 into the inner integral,

$$\Phi \leq \left(\ln \frac{\ell_1}{\ell_2}\right)^{-2} \int_{\ell_2 \lambda_0/c}^{\ell_1 \lambda_0/c} \frac{d\xi}{\xi} \int_{\ell_2 \lambda_0/c}^{\ell_1 \lambda_0/c} \frac{d\xi'}{\xi'} \max_{\tau_1, \tau_2} \gamma'(\tau_1 - \tau_2 + \xi - \xi'). \quad (28)$$

Note that $|\tau_1 - \tau_2| < T$, so

$$\max_{\tau_1, \tau_2} \gamma'(\tau_1 - \tau_2 + \xi - \xi') = G(\xi - \xi'; 2T). \quad (29)$$

Switching to nondimensional form including the dummy variable ξ in the outer integral,

$$\Phi \leq \left(\ln \frac{\ell_1}{\ell_2}\right)^{-2} \int_{\ell_2}^{\ell_1} \frac{d\xi}{\xi} \int_{\ell_2 - \xi}^{\ell_1 - \xi} \frac{d\zeta}{\zeta + \xi} g(\zeta, 2\mu). \quad (30)$$

The order of integration can be switched. Note that because we have not needed to inflate the limits of the inner integral, the picture looks like that in Fig. 5 with the center band in the right-hand panel collapsed. Thus, only two integration regions are required, leading to

$$\Phi \leq \left(\ln \frac{\ell_1}{\ell_2}\right)^{-2} \left[\int_0^{\Delta\ell} d\zeta g(\zeta, 2\mu) \int_{\ell_2}^{\ell_1 - \zeta} \frac{d\xi}{\xi} \frac{1}{\zeta + \xi} + \int_{-\Delta\ell}^0 d\zeta g(\zeta, 2\mu) \int_{\ell_2 - \zeta}^{\ell_1} \frac{d\xi}{\xi} \frac{1}{\zeta + \xi} \right]. \quad (31)$$

Using the results from (24) and (25), this can be integrated to form the alternate bound,

$$\Phi \leq 2 \left(\ln \frac{\ell_1}{\ell_2}\right)^{-2} \int_0^{\Delta\ell} d\zeta g(\zeta, 2\mu) \frac{1}{\zeta} \left(\ln \frac{(\ell_1 - \zeta)(\ell_2 + \zeta)}{\ell_1 \ell_2} \right). \quad (32)$$

REPORT DOCUMENTATION PAGE*Form Approved
OMB No. 0704-0188*

The public reporting burden for this collection of information is estimated to average 1 hour per response, including the time for reviewing instructions, searching existing data sources, gathering and maintaining the data needed, and completing and reviewing the collection of information. Send comments regarding this burden estimate or any other aspect of this collection of information, including suggestions for reducing the burden, to Department of Defense, Washington Headquarters Services, Directorate for Information Operations and Reports (0704-0188), 1215 Jefferson Davis Highway, Suite 1204, Arlington, VA 22202-4302. Respondents should be aware that notwithstanding any other provision of law, no person shall be subject to any penalty for failing to comply with a collection of information if it does not display a currently valid OMB control number.

PLEASE DO NOT RETURN YOUR FORM TO THE ABOVE ADDRESS.

1. REPORT DATE (DD-MM-YYYY)		2. REPORT TYPE		3. DATES COVERED (From - To)	
4. TITLE AND SUBTITLE				5a. CONTRACT NUMBER	
				5b. GRANT NUMBER	
				5c. PROGRAM ELEMENT NUMBER	
6. AUTHOR(S)				5d. PROJECT NUMBER	
				5e. TASK NUMBER	
				5f. WORK UNIT NUMBER	
7. PERFORMING ORGANIZATION NAME(S) AND ADDRESS(ES)				8. PERFORMING ORGANIZATION REPORT NUMBER	
9. SPONSORING/MONITORING AGENCY NAME(S) AND ADDRESS(ES)				10. SPONSOR/MONITOR'S ACRONYM(S)	
				11. SPONSOR/MONITOR'S REPORT NUMBER(S)	
12. DISTRIBUTION/AVAILABILITY STATEMENT					
13. SUPPLEMENTARY NOTES					
14. ABSTRACT					
15. SUBJECT TERMS					
16. SECURITY CLASSIFICATION OF:			17. LIMITATION OF ABSTRACT	18. NUMBER OF PAGES	19a. NAME OF RESPONSIBLE PERSON
a. REPORT	b. ABSTRACT	c. THIS PAGE			19b. TELEPHONE NUMBER (Include area code)